Supporting Online Material for

Two-Dimensional Mott-Hubbard Electrons in an Artificial Honeycomb Lattice

A. Singha, M. Gibertini, B. Karmakar, S. Yuan, M. Polini,* G. Vignale, M. I. Katsnelson, A. Pinczuk, L. N. Pfeiffer, K. W. West, V. Pellegrini*

*To whom correspondence should be addressed. E-mail: vp@sns.it (V.P.); m.polini@sns.it (M.P.)

Published 3 June 2011, *Science* **332**, 1176 (2011)
DOI: 10.1126/science.1204333

This PDF file includes:

Supporting Online Material for "Two-dimensional Mott-Hubbard electrons in an artificial honeycomb lattice"

A. Singha,[1,*] M. Gibertini,[1] B. Karmakar,[1] S. Yuan,[2] M. Polini,[1,3,†] G. Vignale,[4,3]
M.I. Katsnelson,[2] A. Pinczuk,[5] L.N. Pfeiffer,[6] K.W. West,[6] and V. Pellegrini[1,‡]

[1]*NEST, Istituto Nanoscienze-CNR and Scuola Normale Superiore, I-56126 Pisa, Italy*
[2]*Radboud University Nijmegen, Institute for Molecules and Materials, NL-6525 AJ Nijmegen, The Netherlands*
[3]*Kavli Institute for Theoretical Physics China, CAS, Beijing 100190, China*
[4]*Department of Physics and Astronomy, University of Missouri, Columbia, Missouri 65211, USA*
[5]*Department of Applied Physics and Applied Mathematics and Department of Physics , Columbia University New York, USA*
[6]*Department of Electrical Engineering, Princeton University, Princeton, NJ, USA*

NANOFABRICATION OF THE ARTIFICIAL LATTICE AND RESONANT ENHANCEMENT OF LIGHT SCATTERING PEAKS

The in-plane potential modulation is achieved by defining an array of Nickel disks (with diameter $2r$) arranged in a honeycomb-lattice geometry (with lattice constant a) by e-beam nanolithography and then by etching away the material outside the disks by inductive coupled reactive ion shallow etching [1, 2]. Owing to the dependence of band-bending profiles on GaAs cap-layer thickness, the resulting pillars [see Fig. 1A in the main text] induce a lateral potential modulation with an amplitude of a few meV's acting on the electronic system [2]. By tuning the etching depth d we can reach different regimes (*i.e.* different values of V_0). We focus on a sample with $d \sim 60$ nm for which we estimate $V_0 \sim 4$ meV [3].

The resonant inelastic light scattering experiments were performed by using a ring-etalon Ti:Sapphire laser with a tunable wavelength of circa 800 nm in resonance with the magneto-luminescence of the nanostructured semiconductor (data not shown) focused on the array with a 100 μm diameter area. The scattered light was collected into a triple grating spectrometer with CCD detection: for the geometry of the experiment see Fig. 1B in the main text. The intensity of the incident radiation was kept to values well below 10^{-1} W/cm^2 to avoid significant heating of the electrons.

Crucial for the optical detection of the Hubbard and spin modes of the electrons in the honeycomb lattice is the resonant enhancement of the corresponding light scattering cross sections. This occurs when the incoming laser energy matches the energy of an inter-band transition of the host crystal. In the experiment this is achieved by tuning the laser energy and plotting the light scattering signal as a function of energy shift with respect to the laser energy. Examples of the resonant effect for the Hubbard mode and for the spin-wave and spin-flip modes (reported in Figs. 1, 3, and 4 of the main text) can be found in Fig. S1. When displayed as a function of energy shift, the collective modes occur at a fixed energy and their intensities follow a resonant profile.

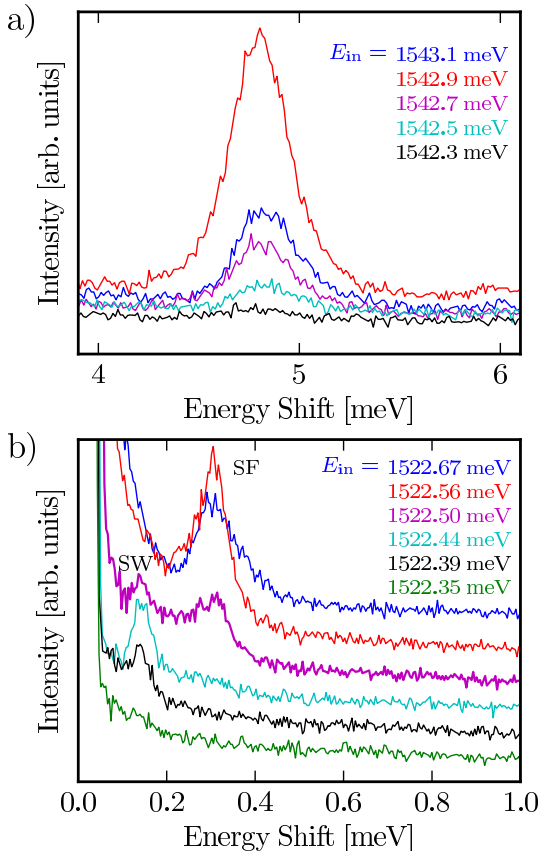

FIG. S1: Resonant profile of inelastic light scattering spectra showing the Hubbard mode at $T = 1.7$ K and $B = 5.48$ T [(panel a)] and the spin-wave (SW) and spin-flip (SF) modes at $T = 55$ mK and $B = 5.48$ T [panel b)]. The incident photon energies are indicated.

LIGHT SCATTERING SPECTROSCOPY OF THE CYCLOTRON MODE

Representative resonant inelastic light scattering spectra at $T = 1.7$ K manifesting the cyclotron mode at two values of the perpendicular magnetic field B are reported in Fig. S2. The cyclotron mode is parity-forbidden in the dipole approximation, and its non-zero albeit weak cross section originates from valence-band mixing effects [4].

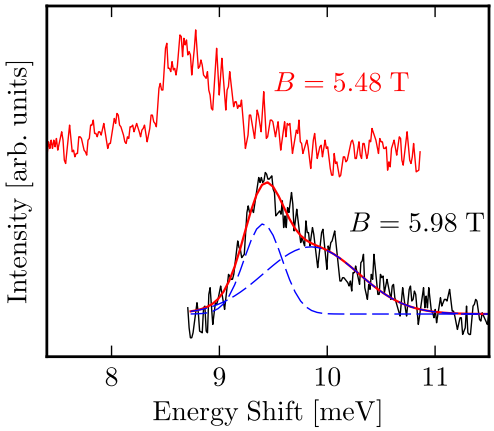

FIG. S2: Representative resonant inelastic light scattering spectra showing the cyclotron mode at $T = 1.7$ K and $B = 5.48$ T and 5.98 T. Incident photon energy is 1547.7 meV and 1546.5 meV, respectively. A fit (red solid line) with two gaussians (blue dashed lines) is also shown.

The fact that we see the *ordinary* 2DEG cyclotron mode in our nanopatterned system is due to a magnetic length ℓ_B that is smaller than the lattice parameters in the explored range of magnetic fields. (The magnetic length ℓ_B at $B = 2$ T is ~ 18 nm, which is smaller than the pillar diameter $2r \sim 60$ nm.) There is a *second* peak above ω_c (the red solid line in Fig. S2 is a fit with two gaussians, which are shown as blue dashed lines) that can be associated to a finite-wavevector excitation due to the dispersion of the cyclotron mode [4] and the optical grating effect of the lattice [5]. The cyclotron mode can be detected for $B \gtrsim 2$ T, a value associated with electrons occupying the lowest Landau level only as indicated by the magneto-transport analysis (data not shown and Ref. 3). We found that its intensity does not vary significantly in the explored range of magnetic fields.

EVALUATION OF THE SCATTERING CROSS SECTION OF THE HUBBARD MODE

In Fig. 2B of the main text we have shown a possible two-photon process that contributes to the scattering cross section of the Hubbard collective mode. In this scheme the initial state $|1\rangle$ is characterized by a pair of neighboring singly-occupied sites with two active electrons in an antiparallel spin configuration. In the final state $|2\rangle$ the two initial electrons occupy the same site. The final excited state is separated from the ground state by the Hubbard charge gap U, *i.e.* by the energy cost of having two antiparallel spin electrons on the same site. Because the lower and upper states split by U have the same parity (as they both emerge from the very same single-particle level at energy ε_0) the process depicted in Fig. 2B of the main text is allowed in the dipole approximation, and its intensity is thus expected to be much larger than the one of the cyclotron mode at ω_c [because of the vanishing of the dynamical structure factor $\mathcal{S}(\omega)$ at ω_c] in agreement with the experimental observation. The scattering cross section can be roughly evaluated in the dipole approximation [6] by assuming that the valence-band holes are not strongly affected by the external periodic modulation. Within the same degree of accuracy used to derive Eq. (3) in the main text, we find that the cross section decays exponentially, *i.e.* $d\sigma/d\Omega' \propto \exp\left[-a^2/(4\ell_B^2)\right]$, for sufficiently large values of B in agreement with the experimental observation.

REDUCING THE ELECTRON DENSITY BY THE PHOTO-DEPLETION TECHNIQUE

The electron density of a modulation-doped quantum well like the one used in our study can be reduced by continuous illumination with photon energy larger than the quantum-well (QW) barrier (≈ 1.6 eV in our case). The mechanism of photo-depletion is based on the fact that photoexcited electrons in the AlGaAs barrier contribute to a charge compensation of the ionized donors while photoexcited holes are swept in the QW region, thereby reducing the electron density through electron-hole radiative recombination [7].

In our studies we used a HeNe laser at energy of 1.96 eV with powers P up to 50 μW. The calibration of electron density versus HeNe power P is obtained by monitoring the evolution of the QW photoluminescence (PL) in an unpatterned region of the sample. Representative spectra are shown in Fig. S3. The QW optical emission exhibits the usual line shape of a modulation-doped QW luminescence, as determined by the recombination of electrons from the bottom of the subband up to the Fermi energy (see inset to the left panel of Fig. S3). The distance between the main PL peak at energy E_1 and the shoulder at energy E_2 is related to the electron density n through the relation $|E_1 - E_2| = E_F(1 + m_e/m_h)$, where $m_{e(h)}$ are the effective masses for electrons (holes) and $E_F = \pi n \hbar^2/m_e$ is the Fermi energy. This relation thus allows us to estimate the electron density n in the unpatterned 2DEG as a function of P. This simple analysis cannot be applied to the patterned region since in this case the PL lineshape is significantly modified as discussed in Ref. 2. The 2DEG density n can be significantly reduced from its zero-power value ($\sim 1 \times 10^{11}$ cm^{-2}) as the HeNe power P is increased.

The right panel in Fig. S3 shows the estimated electron concentration per site at different HeNe powers in the nanopatterned region using the calibration method described above (but starting from the $P = 0$ value of the electron density $\sim 3 - 4 \times 10^{10}$ cm^{-2} of the nanopatterned sample).

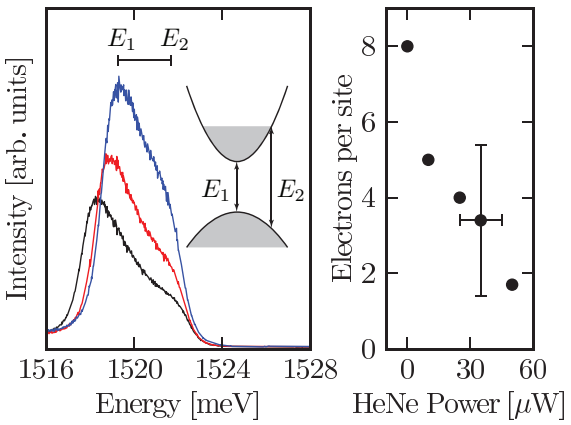

FIG. S3: (Left panel) Evolution of the photoluminescence spectra of the unpatterned 2DEG with varying HeNe power P (black $\rightarrow$ 0 μW; red $\rightarrow$ 10 μW; blue $\rightarrow$ 25 μW). The inset shows a schematic profile of the conduction and valence bands: occupied states are indicated by gray-shaded areas. E_1 and E_2 refer to the main structures in the photoluminescence. (Right panel) Estimated electron concentration per site in the patterned region of the sample *versus* HeNe laser power.

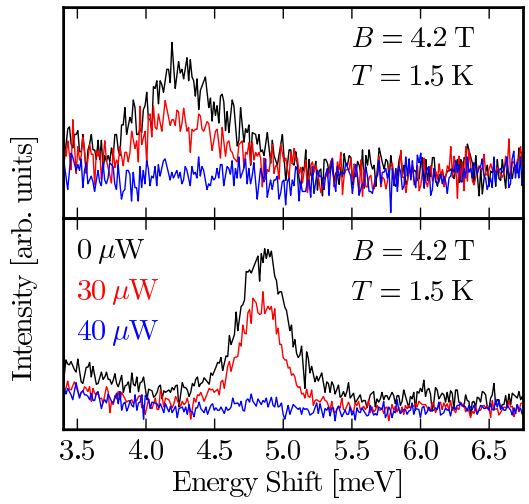

FIG. S4: Representative inelastic light scattering data showing the evolution of the Hubbard mode versus HeNe power at two different magnetic fields. The density is decreased (from black to blue) by means of the photo-depletion technique.

EVALUATION OF DENSITY DEPENDENCE OF THE HUBBARD MODE

In this Section we demonstrate that the Mott-Hubbard gap $\hbar\omega_{\rm HB}$ depends very weakly on the electron concentration in the single-band Hubbard model and in the atomic limit ($U \gg t$).

In the so-called "Hubbard I" approximation [8], which works well at strong coupling, the Hubbard bands $E_\pm(\boldsymbol{k})$ for spin σ electrons are given by the following expression:

$$E_\pm(\boldsymbol{k}) = \varepsilon_0 + \frac{1}{2}\Big[t(\boldsymbol{k}) + U \pm \sqrt{t^2(\boldsymbol{k}) + U^2 + 2t(\boldsymbol{k})U(2n_{-\sigma}-1)}\Big] \quad \text{(S1)}$$

where $t(\boldsymbol{k})$ is the bare band energy and $n_{-\sigma}$ is the concentration of electrons with spin projection opposite to σ. In the atomic limit Eq. (S1) simplifies to

$$\begin{cases} E_+(\boldsymbol{k}) = \varepsilon_0 + U\left[1 + \dfrac{t(\boldsymbol{k})}{U} n_{-\sigma}\right] \\ E_-(\boldsymbol{k}) = \varepsilon_0 + t(\boldsymbol{k})(1 - n_{-\sigma}) \end{cases} . \quad \text{(S2)}$$

We thus immediately see that one band is centered at $\varepsilon_0 + U$ and the other one at ε_0, independently of the electron concentration. The dependence of the Mott-Hubbard gap $\hbar\omega_{\rm HB} \equiv \min_{\boldsymbol{k}}[E_+(\boldsymbol{k}) - E_-(\boldsymbol{k})] = U + \mathcal{O}(t/U)$ on electron concentration is a small effect, of the first order in t/U. In the limit $n_{-\sigma} = 0$ the two Hubbard band energies are at $\varepsilon_0 + t(\boldsymbol{k})$ and $\varepsilon_0 + U$, but the upper band has a vanishing number of states ($n_{-\sigma}$) associated with it. In other words, the strength of the transition from the lower to the upper band vanishes because there are no available states in the upper band.

A similar result is valid also within the multiband generalization of the "Hubbard I" approximation [9]. The Green's function in the strongly-correlated limit is determined by the equation

$$G^{-1}(E, \boldsymbol{k}) = G_{\rm at}^{-1}(E) - t(\boldsymbol{k}) \ , \quad \text{(S3)}$$

where $G_{\rm at}(E)$ is the energy-dependent Green's function of the atomic problem. One can prove (see the Appendix in the work by Lebegue *et al.* [9]) that this expression is exact for the multiband Hubbard model up to first order in t/U. The poles of this function, which determine the positions of the centers of the Hubbard bands, do not depend on electron concentration, while the residues, which determine the width of the Hubbard bands, do.

These theoretical arguments are fully consistent with the experimental observations shown in Fig. 3B of the main text and in Fig. S4.

TIGHT-BINDING CALCULATIONS IN THE ULTRA-HIGH-MAGNETIC-FIELD REGIME

We have performed extensive tight-binding calculations of the density-of-states (DOS) of non-interacting electrons hopping on a honeycomb lattice in the presence of a perpendicular magnetic field B and of uniformly-distributed disorder of amplitude W. We have simulated both on-site disorder, which is mathematically described by an Hamiltonian of the type

$$\hat{\mathcal{H}}_{\rm dis} = \sum_i \varepsilon_i \hat{n}_i \quad \text{(S4)}$$

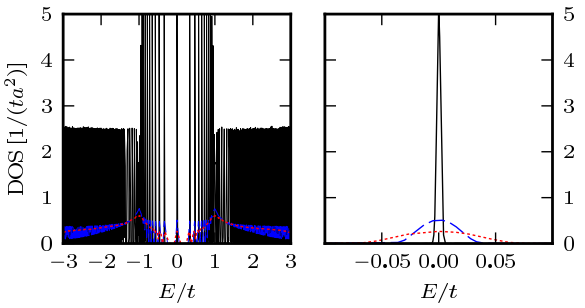

FIG. S5: Calculated DOS [in units of $1/(ta^2)$] as a function of energy E (in units of t) for electrons hopping on a honeycomb lattice with lattice constant $a = 130$ nm and in the presence of a small magnetic field $B = 0.001$ T. We clearly see the zero-energy Landau level, unevenly spaced Landau levels of massless Dirac fermions at low energies, and equally spaced ordinary Landau levels at higher energies. The panel on the right is a zoom of the low-energy sector. Black lines label the DOS of the clean system, while blue dashed ($W = 0.5\ t$) and red dotted ($W = 1.0\ t$) lines label results for the disordered system. Data for $W \neq 0$ have been obtained by using random on-site disorder, see Eq. (S4). These numerical results have been obtained by using periodic boundary conditions on a sample containing 3200×3200 lattice sites.

with ε_i uniformly distributed in the interval $[-W/2, +W/2]$ and disorder due to random hopping, which is described by an Hamiltonian of the type

$$\hat{\mathcal{H}}'_{\rm dis} = \sum_{\langle i,j \rangle} \delta t_{ij} \hat{c}_i^\dagger c_j \qquad \text{(S5)}$$

where δt_{ij} is uniformly distributed in the interval $[-W/2, +W/2]$. Details on the numerical technique can be found *e.g.* in Ref. 10.

In Figs. S5-S6 we collect our main findings for a honeycomb lattice with $a = 130$ nm and B varying from 0.001 T up to 5 T.

In Fig. S5 we clearly see that when $\ell_B > a$ the calculated DOS is indistinguishable from that of graphene and exhibits a zero-energy Landau level and massless Dirac fermions at low energies stemming from the topology of the lattice [11, 12]. When disorder is switched on, the zero-energy Landau level broadens. Fig. S5 illustrates the DOS in the ultra-high-magnetic-field regime, *i.e.* for $\ell_B < a$. For $B = 2$ T and 5 T, for example, we clearly see that, in the absence of disorder, a series of Hofstadter states appears near zero energy due to commensurability effects [13–15] (*i.e.* the magnetic flux $\Phi = 3\sqrt{3}a^2B/2$ through the unit cell of the honeycomb lattice being of the same order of the quantum flux unit hc/e). When disorder is taken into account a broad structure near zero energy emerges akin to the zero-energy Landau level in disordered graphene (see right panel in Fig. S5). Notice that this structure has a width in energy of the order of

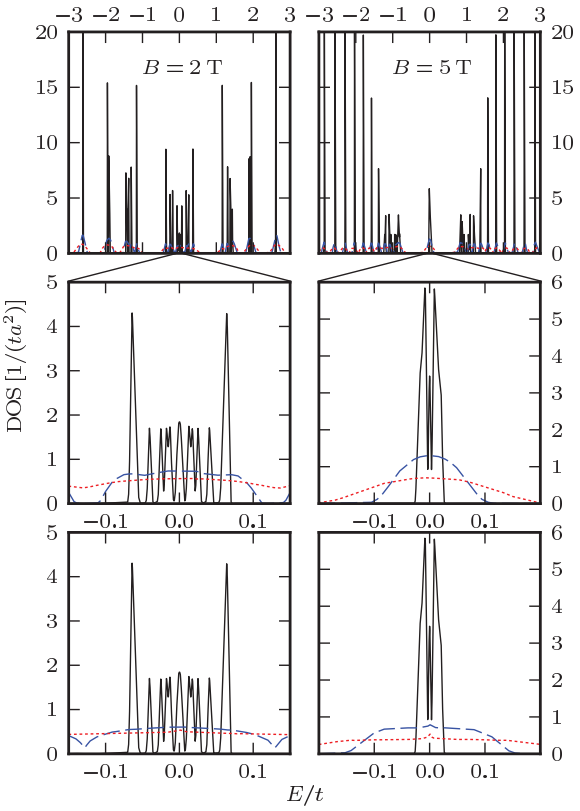

FIG. S6: Same as in Fig. S5 but for higher values of the magnetic field, $B = 2$ T (left panels) and $B = 5$ T (right panels). Color coding and labeling are the same as in Fig. S5. Data for $W \neq 0$ in the two panels at the bottom have been obtained by using disorder due to random hopping, see Eq. (S5).

0.2 t for $W = 0.5\ t$, *i.e.* roughly twice the width of the zero-energy Landau level in graphene for the same value of W.

In analogy to what observed experimentally in graphene [16–19], we expect that electron-electron interactions can strongly re-organize this low-energy sector yielding a correlated ground state with an energy gap of the order of the spin-doublet energy splitting Δ introduced in the main text. Similarly to graphene [19], the precise mechanism responsible for the emergence of this novel ground state is, to date, unknown. A broken-symmetry ground state driven by lattice-scale interactions beyond the continuum model is compatible with the experimental results [20].

Before concluding, we would like to emphasize that in the limit in which ℓ_B is smaller than a effects beyond those captured by the tight-binding model should be taken into account since the shape of the "atomic orbitals" is altered. To a first approximation, the magnetic field simply increases the confinement of electrons

in each minimum of the periodic potential ("magnetic squeezing") thereby renormalizing the hopping amplitude $|t| \to |t(B)|$. In the clean limit this fact has no implications on the validity of our results in Figs. S5-S6. Indeed, the data reported in these plots illustrate the DOS [in units of $1/(ta^2)$] as a function of E/t: the hopping amplitude is the only energy scale and its precise value thus does not matter.

In the presence of disorder, however, as magnetic field B increases, the tendency to Anderson localization increases too. The actual phase diagram (and broken-symmetry states) of the nanopatterned electron gas results from the competition between electron-electron interactions, disorder, and external periodic potential. This is clearly beyond the scope of the elemental theoretical analysis reported in the main text and in the SOM and is left for future investigations. The experimental data in Fig. 4 of the original manuscript strongly suggest that electron-electron interactions are capable of re-organizing the low-energy degrees of freedom of the nanopatterned electron liquid at least up to magnetic field values of the order of 8-9 Tesla.

* Present address: Department of Physics, Bose Institute, 93/1 Acharya Prafulla Chandra Road, Kolkata 700009, India.
† Electronic address: m.polini@sns.it
‡ Electronic address: vp@sns.it

[1] C.P. Garcia, V. Pellegrini, A. Pinczuk, M. Rontani, G. Goldoni, E. Molinari, B.S. Dennis, L.N. Pfeiffer, K.W. West, *Phys. Rev. Lett.* **95**, 266806 (2005).
[2] M. Gibertini, A. Singha, V. Pellegrini, M. Polini, G. Vignale, A. Pinczuk, L.N. Pfeiffer, K.W. West, *Phys. Rev. B* **79**, 241406(R) (2009).
[3] G. De Simoni, A. Singha, M. Gibertini, B. Karmakar, M. Polini, V. Piazza, L.N. Pfeiffer, K.W. West, F. Beltram, V. Pellegrini, *Appl. Phys. Lett.* **97**, 132113 (2010).
[4] A. Pinczuk, B.S. Dennis, D. Heiman, C. Kallin, L. Brey, C. Tejedor, S. Schmitt-Rink, L.N. Pfeiffer, K.W. West, *Phys. Rev. Lett.* **68**, 3623 (1992).
[5] L.L. Sohn, A. Pinczuk, B.S. Dennis, L.N. Pfeiffer, K.W. West, L. Brey, *Solid State Commun.* **93**, 897 (1995).
[6] V.B. Berestetskii, E.M. Lifshitz, L.P. Pitaevskii, *Quantum Electrodynamics* (Pergamon Press, Oxford, 1982), Chapter VI.
[7] I.V. Kukushkin, K. von Klitzing, K. Plogg, V.E. Kirpichev, B.N. Shepel, *Phys. Rev. B* **40**, 4179 (1989); J.G. Michels, R.J. Nicholas, G.M. Summers, D.M. Symons, C.T. Foxon, J.J. Harris, *Phys. Rev. B* **52**, 2688 (1995); A.J. Shields, S.L. Osborne, M.Y. Simmons, D.A. Ritchie, M. Pepper, *Semicond. Sci. Technol.* **11**, 890 (1996).
[8] J. Hubbard, *Proc. R. Soc. A* **276**, 238 (1963).
[9] J. Hubbard, *Proc. R. Soc. A* **285**, 542 (1965); A.I. Lichtenstein, M.I. Katsnelson, *Phys. Rev. B* **57**, 6884 (1998); S. Lebegue, G. Santi, A. Svane, O. Bengone, M.I. Katsnelson, A.I. Lichtenstein, O. Eriksson, *Phys. Rev. B* **72**, 245102 (2005).
[10] S. Yuan, H. De Raedt, M.I. Katsnelson, *Phys. Rev. B* **82**, 115448 (2010).
[11] J.W. McClure, *Phys. Rev.* **104**, 666 (1956).
[12] For a review see *e.g.* M.I. Katsnelson, K.S. Novoselov, *Solid State Commun.* **143**, 3 (2007).
[13] F.H. Claro, G.H. Wannier, *Phys. Rev. B* **19**, 6068 (1979).
[14] A.H. MacDonald, *Phys. Rev. B* **29**, 3057 (1984).
[15] R. Rammal, *J. Physique* **46**, 81 (1985).
[16] Y. Zhang, Z. Jiang, J.P. Small, M.S. Purewal, Y.W. Tan, M. Fazlollahi, J.D. Chudow, J.A. Jaszczak, H.L. Stormer, P. Kim, *Phys. Rev. Lett.* **96**, 136806 (2006).
[17] J.G. Checkelsky, L. Li, N.P. Ong, *Phys. Rev. Lett.* **100**, 206801 (2008).
[18] A.J.M. Giesbers, L.A. Ponomarenko, K.S. Novoselov, A.K. Geim, M.I. Katsnelson, J.C. Maan, U. Zeitler, *Phys. Rev. B* **80**, 201403 (2009).
[19] For a recent review see *e.g.* D.S.L. Abergel, V. Apalkov, J. Berashevich, K. Ziegler, T. Chakraborty, *Adv. Phys.* **59**, 261 (2010).
[20] J. Alicea, M.P.A. Fisher, *Phys. Rev. B* **74**, 075422 (2006).